

Claude Bédard¹, Serafim Rodrigues¹, Noah Roy², Diego Contreras² and
Alain Destexhe¹

Evidence for frequency-dependent extracellular impedance from the transfer function between extracellular and intracellular potentials

May 29, 2019

Abstract We examine the properties of the transfer function $F_T = V_m/V_{LFP}$ between the intracellular membrane potential (V_m) and the local field potential (V_{LFP}) in cerebral cortex. We first show theoretically that, in the linear regime, the frequency dependence of the extracellular medium and that of the membrane potential have a clear incidence on F_T . The calculation of F_T from experiments and the matching with theoretical expressions therefore potentially allows one to estimate the impedance of the extracellular medium without injecting currents. We examine the transfer function for bipolar (differential) LFPs and compare to simultaneous recordings of V_m and V_{LFP} in rat barrel cortex *in vivo*. The experimentally derived F_T matches the one derived theoretically, only if one assumes that the impedance of the extracellular medium is frequency-dependent, and varies as $1/\sqrt{\omega}$ (Warburg impedance) for frequencies between 10 and 500 Hz. This constitutes indirect evidence that the extracellular medium is non-resistive, which has many possible consequences for modeling LFPs.

Keywords: *Computational models; Local Field Potentials; EEG; Extracellular resistivity; Intracellular Recordings; Maxwell Equations*

1 Introduction

There is a widespread consensus that mechanisms for generating the intracellular electrical activity are very well understood, however not complete. In contrast, the study of extracellular activity remains mostly illusive and is a subject of intense research. This is associated to the difficulty in assigning measurements of the extracellular potentials to a unique neurophysiological generator, which makes modeling of LFP/EEG a complex issue. Some of these

mechanisms are believed to be related to synaptic activity, synchronous population spikes, ephaptic interaction, ionic dynamics, morphological structure of the neurons and many other processes (reviewed in [Jefferys (1995), Nunez and Srinivasan (2006)]).

One of the characteristics of extracellular potentials is the very steep attenuation of “fast” events such as spikes, which are visible only within the immediate vicinity (a few microns) of the electrode. In contrast, “slow” events such as synaptic potentials are visible for much larger distances, typically a few hundred microns [Destexhe *et al.* (1999), Katzner *et al.* (2009)]. One way to explain this differential filtering is that the extracellular medium acts as a powerful low-pass filter [Bédard *et al.* (2004)]. However, this aspect is controversial because some measurements of brain conductivity did not display significant filtering effects [Logothetis *et al.* (2001)] while other measurements did [Ranck (1963), Gabriel *et al.* (1996)]. However, these measurements tend to use currents that are much larger than biological sources, which may explain the discrepancy [Bédard and Destexhe (2009)].

In the present paper, we provide theoretical work and analyze experimental measurements to examine whether the extracellular medium is non-resistive. In particular, we examine a quantity which depends on the extracellular impedance, the transfer function between simultaneously recorded intracellular and extracellular potentials. We show theoretically that, in the linear regime and for point current sources, this transfer function strongly depends on the extracellular impedance, and can therefore be used to investigate its frequency dependence. In addition we show preliminary results from *in vivo* recordings, which indicate that the extracellular medium is indeed frequency dependent. This point source model is the simplest possible, however it explains the broad features of the data in parsimonious way. This finding has many possible implications for modelling LFPs/EEG.

1: Integrative and Computational Neuroscience Unit (UNIC),
UPR2191, CNRS, Gif-sur-Yvette, France
E-mail: Destexhe@unic.cnrs-gif.fr

2: Department of Neuroscience, University of Pennsylvania,
Philadelphia, USA.

2 Methods

2.1 Surgery and Preparation

Experiments were conducted in accordance with the ethical guidelines of the National Institutes of Health and with the approval of the Institutional Animal Care and Use Committee of the University of Pennsylvania. Adult male Sprague-Dawley rats (300-350g, $n=35$) were anesthetized with isoflurane (5% for induction, 2% during surgery), paralyzed with gallamine triethiodide, and artificially ventilated. End tidal CO₂ (3.5-3.7%) and heart rate were continuously monitored. Body temperature was maintained at 37°C via servo-controlled heating blanket and rectal thermometer (Harvard Apparatus, Holliston, MA). The rat was placed in a stereotaxic apparatus and a craniotomy was made directly above both the barrel cortex (1.0-3.0 mm A/P, 4.0-7.0 mm M/L) and the medial ventroposterior thalamic nucleus (VPm, 3.0 mm A/P, 3.0 mm M/L), and the dura was resected. The cisterna magna was drained to improve stability. For intracellular recordings, additional measures were taken to improve stability, including dexamethasone (10 mg/kg, i.p.) to reduce brain swelling, hip suspension, and filling the craniotomy with a solution of 4% agar.

2.2 Electrophysiological Recordings

Recordings of local field potentials (LFPs) across the cortical depth were performed with 16-channel silicon probes (Neuronexus, Ann Arbor, MI). Probe recording sites were separated by 100 μ m and had impedances of 1.5-2.0 M Ω at 1 kHz. The probe was lowered into the brain under visual guidance, oriented normal to the cortical surface, until the most superficial recording site was aligned with the surface (see Fig. 1). LFP signals were amplified and filtered at 0.1 Hz–10 kHz (FHC, Inc., Bowdoinham, ME).

Intracellular recordings from barrel cortex were performed with glass micropipettes pulled on a P-97 Brown Flaming puller (Sutter Instrument Company, Novato, CA). Pipettes were filled with 3M potassium acetate and had DC resistances of 60-80 M Ω . A high-impedance amplifier (low-pass filter of 5 kHz) with active bridge circuitry (Neurodata, Cygnus Technology, Inc., Delaware Water Gap, PA) was used to record and inject current into cells. Vertical depth was measured by the scale on the micromanipulator. A Power 1401 data acquisition interface and Spike2 software (Cambridge Electronic Design, Cambridge, U.K.) were used for data acquisition and online averaging.

2.3 Analysis and simulations

All simulations and analyses were realized using MATLAB (Mathworks Inc, Natick, MA).

3 Theory

In this section we formulate a theoretical relationship between extracellular and intracellular sub-threshold voltage activity. In particular, the formulation is performed in the frequency domain to easily allow comparisons between the amount of intracellular and extracellular signal within each frequency band across different frequency ranges, which is readily accessible from experimental data. The advantage of this approach is simplicity as it avoids tackling directly the different time scales dynamics inherently associated to LFP/EEG signals, many of which are not yet understood. For example, it is known that LFP/EEG signals are composed of mixed-mode oscillations, however the origins and transitions between these modes are not yet explained [Erchova and McGonigle (2008)]. To circumvent these theoretical time domain issues we establish this theory in the frequency space. This choice also seems natural because the differential equations describing electric potentials transform into algebraic equations in frequency space.

The formulation of the relation between transmembrane (V_m) and extracellular (V_{LFP}) activity requires to first derive the transfer function, F_T , that measures the ratio between the impedance of the cellular membrane and extracellular medium. For sake of completeness, we begin with the simplest case scenario of a single neuronal source. However, future considerations should address more complex cases, including super-threshold activity. Thus we will assume a single source forming a monopole with spherical symmetry and spherical iso-potential surfaces. The source observable V_m is decomposed as the difference between the potentials at each side of the membrane, V_i and V_e , as indicated in Fig. 1A. In addition, we will assume an isotropic and homogeneous extracellular medium (but not necessarily resistive). We note that the derivations herein developed are similar for planar and cylindrical symmetry.

In the following, we use the notation $F(\omega)$ to denote the function F in Fourier space, with $\omega = 2\pi f$ where f is the frequency.

3.1 Membrane impedance for a spherical source in the linear regime

We assume that the extracellular electric field is produced by a spherical source embedded in a medium which is homogeneous/isotropic and continuous, and with electric pa-

rameters σ_ω , ε_ω ¹. The cell is represented by an RC circuit where the membrane potential is expressed as the difference $V_m = V_e - V_i \approx -70 \text{ mV}$ (Fig. 1A). At rest, there is a net negative charge Q_- inside, which is perfectly balanced with a net positive charge Q_+ on the external surface of the membrane, such as $Q_- + Q_+ = 0$. In this situation, the electric field \mathbf{E} produced by the cell in the medium is null, which implies that $V_e = R_f^\infty = 0$, where R_f^∞ is the reference potential at infinite distance from the source.

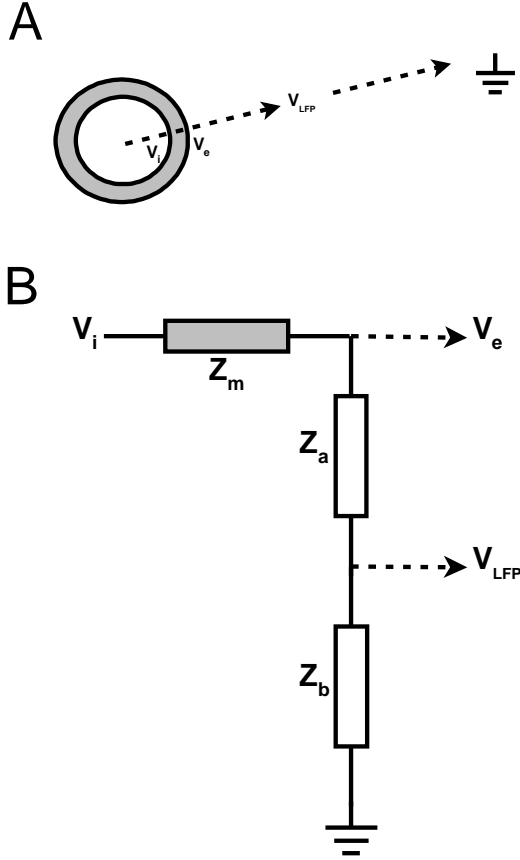


Fig. 1 Arrangement of potentials and impedances for a spherical source. A. Scheme of the spherical source and the different potentials used for calculations. We assume that the extracellular medium is homogeneous, so that there is no position-dependence of conductivity or permittivity. V^i and V^e are the electric potentials, respectively inside and outside of the membrane, relative to a reference potential $R_f^\infty = 0$ situated at an infinite distance. V_{LFP} is the local field potential, which is the voltage difference between a point P in extracellular space and R_f^∞ . B. Equivalent electrical circuit for this configuration, where Z_m is the impedance of the membrane, while Z_a and Z_b are impedances of the extracellular medium.

Suppose that a small excess of positive charge is injected inside the cell. Due to this excess of charge, an electric field \mathbf{E} will instantaneously appear in extracellular space. There will also be production of an electric current to re-

store the equilibrium (and therefore a variation of the electric field). The current produced depends on the physical and biological characteristics of the membrane, which will determine the time evolution of the electric field. The current is given by:

$$\begin{aligned} I_r &= \sum_{i=1}^N g_i(t, V_m)(V_m(t) - E_i) \\ I_c &= C_m \frac{dV_m}{dt} \\ I_m &= I_r + I_c \end{aligned} \quad (1)$$

where I_r and I_c are the ionic and capacitive currents, respectively. The index i represents the different membrane conductances g_i , with their reversal potential E_i , and C_m is the membrane capacitance.

In the following, we will assume that the excess of charge remains small and varies around a stationary mean value, so that we can neglect the time variations of conductances and of the V_m (ΔV_m), with $\partial g_i^j / \partial V_m \approx 0$. In this case, we can consider that the conductances are only function of the mean value of the V_m . This is equivalent to assume that, in the subthreshold regime, the conductances are not dependent on the potential, and that the reversal potentials E_i are constant. This is valid if the impact of ionic concentration changes on E_i are negligible compared to the voltage variations.

Under these approximations, we can write:

$$\begin{aligned} \Delta I_r &= \sum_{i=1}^N g_i(\langle V_m \rangle_t) \Delta V_m \\ \Delta I_c &= C_m \frac{d\Delta V_m}{dt} \\ \Delta I_m &= \Delta I_r + \Delta I_c \end{aligned} \quad (2)$$

$$\Delta I_m = \Delta I_r + \Delta I_c \quad (3)$$

Here, we have a linear system of equations with time-independent coefficients. By expressing the variation of current produced by the cell as a function of the variation of membrane voltage, in Fourier space, we obtain:

$$\begin{aligned} \Delta I_r(\omega) &= G_m \Delta V_m(\omega) \\ \Delta I_c(\omega) &= i\omega C_m \Delta V_m(\omega) \\ \Delta I_m(\omega) &= \Delta I_r(\omega) + \Delta I_c(\omega) \end{aligned} \quad (4)$$

¹ Note that we keep the electric parameters frequency dependent, to keep the expressions as general as possible. In addition, the theory can easily be generalized to multipoles, as any multipole configuration can be decomposed in a sum of monopoles, and to multiple sources using the linear superposition principle.

where

$$G_m = \sum_{i=1}^N g_i.$$

The impedance of the membrane is given by:

$$Z_m(\omega) = \frac{\Delta V_m(\omega)}{\Delta I(\omega)} = \frac{R_m}{1 + i\omega\tau_m} \quad (5)$$

where $R_m = \frac{1}{G_m}$.

3.2 Computing the transfer function $F_T^{(1)}$

$F_T^{(1)} = \frac{V_m(\omega)}{V_e(\omega)}$ can be calculated from the equivalent circuit shown in Fig. 1B. We have the following relations:

$$\begin{aligned} Z_{med} &= Z_a + Z_b \\ V_m(\omega) &= V_i(\omega) - V_e(\omega) \\ \frac{V_i(\omega)}{Z_m + Z_{med}} &= \frac{V_e(\omega)}{Z_{med}} \end{aligned} \quad (6) \quad (7) \quad (8)$$

It follows that

$$F_T^{(1)} = \frac{V_m(\omega)}{V_e(\omega)} = \frac{Z_m}{Z_{med}} \quad (9)$$

3.3 Computing the transfer function $F_T^{(2)}$

$F_T^{(2)} = \frac{V_e(\omega)}{V_{LFP}(\omega)}$ can also be calculated based on the equivalent circuit of Fig. 1B:

$$F_T^{(2)} = \frac{V_e(\omega)}{V_{LFP}(\omega)} = \frac{Z_a + Z_b}{Z_b} \quad (10)$$

We note that if Z_a and Z_b have the same frequency dependence, for example f^n , then $F_T^{(2)}$ is independent of frequency when the medium is macroscopically homogeneous. For example, if both media have a Warburg impedance ($Z \sim 1/\sqrt{\omega}$) or capacitive impedance ($Z \sim 1/\omega$), the function $F_T^{(2)}$ has the same value as for the case of a resistive medium (frequency independent impedance). For a spherical source, we have:

$$F_T^{(2)} = \frac{V_e(\omega)}{V_{LFP}(\omega)} = \frac{d}{R} \quad (11)$$

because the resistance of a spherical shell of radius r up to infinite equals $\frac{1}{4\pi\sigma r}$, which corresponds to the sum $Z_a + Z_b$ when $r = R$ and Z_b when $r = d$.

In the case of a heterogeneous isotropic medium, we have [Bédard and Destexhe (2009)]:

$$Z(r, \omega) = \frac{1}{4\pi\sigma_z(R)} \int_r^\infty dr' \frac{1}{r'^2} \frac{\sigma_\omega(R) + i\omega \epsilon_\omega(R)}{\sigma_\omega(r') + i\omega \epsilon_\omega(r')} \quad (12)$$

for a spherical and isopotential source. σ_z represents the complex conductivity and r is the distance to the center of the source. In the absence of spherical symmetry and with non-isopotential sources, it is necessary, in general, to solve differential equations derived from Maxwell equations in the quasi-static regime (neglecting electromagnetic induction; see [Chari and Salon (1999)]).

3.4 Frequency dependence of differential (bipolar) recordings

When we have the PSD of LFPs which depends on frequency as $1/f^\gamma$ where $\gamma \geq 1$ (for monopolar LFP recordings), then the energy associated to the signal is necessarily infinite, which is of course physically impossible. In fact, the correct dependence should be of the form

$$V(\omega) = \frac{\kappa_i}{\omega^{\gamma/2} + a_i} = \frac{\frac{\kappa_i}{\sqrt{2\pi}}}{f^{\gamma/2} + \frac{a_i}{\sqrt{2\pi}}} \quad (13)$$

Note that the PSD is proportional to the square of $V(\omega)$ and will thus scale as $1/f^\gamma$ in this case.

The values of constants κ_i and a_i represent respectively the proportionality constant for each electrode i , which depends on the intensity of the field for large frequencies, and the natural limit of the value of the voltage for very low frequencies (which limits the energy of the system). In general, these constants depend on electrode position, and therefore when one takes the difference between two electrodes, we have:

$$V_{diff}(\omega) = V_{LFP}^{(1)}(\omega) - V_{LFP}^{(2)}(\omega) = \frac{\kappa_1}{\omega^{\gamma/2} + a_1} - \frac{\kappa_2}{\omega^{\gamma/2} + a_2} \quad (14)$$

If the signal intensities of the two electrodes are comparable for large frequencies, we have necessarily $\kappa_1 \approx \kappa_2$, such that the bipolar signal will have the following form:

$$V_{diff}(\omega) \approx \kappa_1 \cdot \frac{a_2 - a_1}{(\omega^{\gamma/2} + a_2)(\omega^{\gamma/2} + a_1)} \approx \frac{\hat{\kappa}}{\omega^\gamma} \quad (15)$$

where $\hat{\kappa} = \kappa_1(a_2 - a_1)$ and for large frequencies. Thus, if monopolar LFPs have a PSD which varies as $1/f^\gamma$, one can have a PSD in $1/f^{2\gamma}$ in bipolar recordings.

4 Numerical simulations

In this section, we present simple numerical simulations to illustrate how the transfer function is influenced by the frequency dependence of the cellular membrane, that of the medium, and of the recording configuration.

4.1 Resistive membrane with homogeneous/isotropic resistive medium

As a first and simplest case, suppose we have a resistive membrane (the membrane capacitance is neglected), embedded in a homogeneous resistive medium. In this case, the resistive medium is described by Laplace equation, and we have:

$$F_T = F_T^{(1)} \cdot F_T^{(2)} = \frac{R_m}{R_{med}} \cdot \frac{R}{d}, \quad (16)$$

where R is the radius of the source, R_m is the membrane resistance, R_{med} is the resistance of the medium, and d is the distance from the LFP measurement site to the center of the source.

This case, however, is not very realistic because the membrane capacitance is neglected. In the following sections, we consider more elaborate membranes and different extracellular media.

4.2 Capacitive effects of membranes in homogeneous/isotropic resistive media

We now consider a membrane with capacitive effects described by a simple RC circuit, together with a resistive medium. In this case, we have:

$$F_T = F_T^{(1)} \cdot F_T^{(2)} = \frac{Z_m}{R_{med}} \cdot \frac{R}{d}, \quad (17)$$

where the parameters are as described above, with Z_m the membrane impedance. Thus, according to Eq. 5, we have the following transfer function:

$$F_T^S = \frac{R_m}{R_{med}} \cdot \frac{1}{1 + i\omega\tau_m} \cdot \frac{R}{d}. \quad (18)$$

This transfer function is depicted in Fig. 2a.

The transfer function can also be calculated for a “non ideal” membrane, with a more realistic RC circuit model where the capacitance is non-ideal and does not charge instantaneously (see details in [Bédard and Destexhe (2008)]; see also Appendix). Considering such a non-ideal membrane with a resistive medium, we have:

$$F_T^N = \frac{R_m}{R_{med}} \cdot \frac{1}{1 + i\frac{\omega\tau_m}{1+i\omega\tau_{MW}}} \cdot \frac{R}{d}. \quad (19)$$

Note that when $\tau_{MW} = 0$ we recover the case above for an ideal membrane. This transfer function is represented in Fig. 2b. The transfer function is in general monotonic (and scales close to $1/f^2$). Interestingly, there is a phase resonance for non-ideal membranes (see (\star) in Fig. 2b).

4.3 RC membrane in homogeneous/isotropic non-resistive medium

We now focus on non-resistive media by providing a transfer function for which the functional form should be observable from extracellular measurements. We consider the simplest case scenario of only linear subthreshold regime where the membrane is described by a simple RC circuit embedded in a medium with impedance $Z(\omega)$. In this case, the transfer function for a mono-polar extracellular recording is given by:

$$F_T = R_m \cdot \frac{1}{Z(\omega) (1 + i\omega\tau_m)} \cdot \frac{R}{d}, \quad (20)$$

If the impedance of the medium is a Warburg type impedance $\kappa/\sqrt{\omega}$ [Bédard *et al.* (2004)], where κ is a complex constant, the transfer function becomes:

$$F_T = \frac{R_m}{\kappa} \cdot \frac{\sqrt{\omega}}{1 + i\omega\tau_m} \cdot \frac{R}{d}. \quad (21)$$

In Fig. 2c, we show few examples of such a case with different values of the membrane time constant τ_m . We observe that the modulus of the transfer function can present a maximum which depends on τ_m , and therefore of the level of activity or the “conductance state” of the membrane.

5 Comparison with experimental results

In this section, we test the resistive or non-resistive nature of the extracellular medium by evaluating the transfer function from experimental data and compare with theoretical estimates. However, we note that in our experiments we use bipolar LFPs recorded in rat barrel cortex, simultaneously with intracellular recordings in the same cortical area. Since the LFP recordings are bipolar, it turns out that we can not directly use Eq. 21 which is valid only for monopolar recordings. Instead, for the bipolar montage we have the following transfer function for large frequencies (for details, see Section 3.4):

$$F_T^{(diff)} = \frac{R_m \omega^\gamma}{\hat{\kappa} (1 + i\omega\tau_m)} \cdot \frac{R}{d}, \quad (22)$$

with $Z(\omega) = \frac{\kappa_i}{\omega^{\gamma/2 - a_i}}$ and $\gamma \geq 1$. Here, R_m is the membrane resistance, τ_m the membrane time constant, $\hat{\kappa}$ a constant

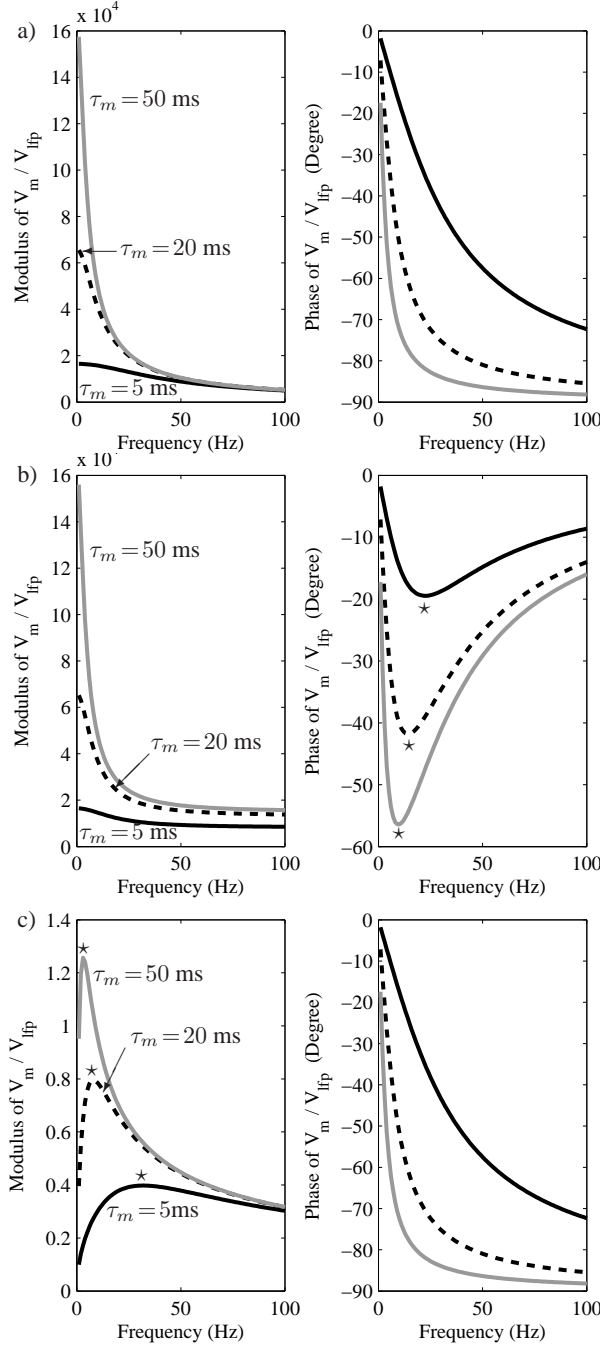


Fig. 2 Amplitude and phase of the transfer function F_T as a function of frequency for different models and for mono-polar electrode montage. In all cases the transfer function was estimated for a distance of $30 \mu\text{m}$ from a spherical source of $10 \mu\text{m}$ radius. A. Standard RC membrane model with $C_m = 10^{-2} \text{ F/m}^2$ and various configurations for membrane time constant τ_m . The extracellular medium conductivity is 0.3 S/m . B. Non-ideal membrane model (see [Bédard and Destexhe (2008)]) with same parameters as in A, and with a Maxwell-Wagner time $\tau_{MW} = 5 \text{ ms}$ (see Appendix). The extracellular medium is also resistive in this case. Surprisingly, we observe a resonance in the phase of the transfer function as indicated by (*). C. Standard RC membrane model together with a medium described by a Warburg Impedance. Note that there is a peak in amplitude of the absolute value of the transfer function that increases and shifts to lower frequencies as τ_m increases; * indicates a resonance.

(see Eq. 15), R the radius of the source, and d is the distance between the recording site and the source (approximately 1 mm in these experiments).

In the particular case of a Warburg impedance ($\gamma = 1$), we have:

$$F_T^{(diff)} = \frac{R_m}{\hat{\kappa}} \cdot \frac{\omega}{1 + i\omega\tau_m} \cdot \frac{R}{d}, \quad (23)$$

while for a quasi-resistive medium $Z(\omega) = \frac{\kappa_i}{\omega^\gamma - a_i}$ with γ very close to zero, and where κ is a constant, we have:

$$F_T^{(diff)} = \frac{R_m}{\hat{\kappa} (1 + i\omega\tau_m)} \cdot \frac{R}{d}, \quad (24)$$

We now compare Eqs. 23-24 with the experimental measurements. We have analyzed four neurons in which simultaneous V_m and (bipolar) V_{LFP} were obtained from rat barrel cortex *in vivo*. Because the theoretical estimates are for linear regime activity, our analysis must avoid any possible interference with spikes, and focus solely on long periods of subthreshold activity as marked by the grey shaded boxes superimposed on the V_m and LFP traces (see Fig. 3). The bottom panels of Fig. 3 show the PSD of the V_m and of V_{LFP} , which display similar slopes.

To compute the transfer function from these data sets, we evaluated the ratio of the calculated PSD (power spectra) of V_m and LFP as shown in Fig. 4a, which corresponds to the data of Fig. 3. As suggested by this similar scaling (bottom panel of Fig. 3, the transfer function of the data $F_T^{(diff)}$ has a mean value that is approximately constant (slope zero) for a large frequency range (Fig. 4a-b). In addition, we performed a constrained nonlinear least square fit for both the transfer function (Eq. 23 and Eq. 18) to the calculated data transfer function $F_T^{(diff)}$. The parameters of the transfer functions were constrained to physiological range. These fits are shown by black line (for Warburg-type media) and dark grey line (for Resistive type media) (within 10 and 500 Hz) in Fig. 4a-b. The matching of this transfer function with different templates shows that, for frequencies between 10 and 500 Hz, a Warburg impedance best accounts for the observed transfer function (Fig. 4a-b). We note that the fit for a resistive-type medium given by Eq. 18 always reached the boundaries of the constrained fit, which is indicative that the obtained minimum in parameter space is far from optimal. To confirm this, we allowed an unconstrained parameter fit and we observed that although the resistive-type would seemingly improve the fit (i.e. the initial plateau of the resistive-type curve would shift towards the 10-500 Hz range), it would however provide unrealistic parameter ranges.

6 Discussion

In this paper, we have examined the transfer function between intracellular and extracellular potentials. The main

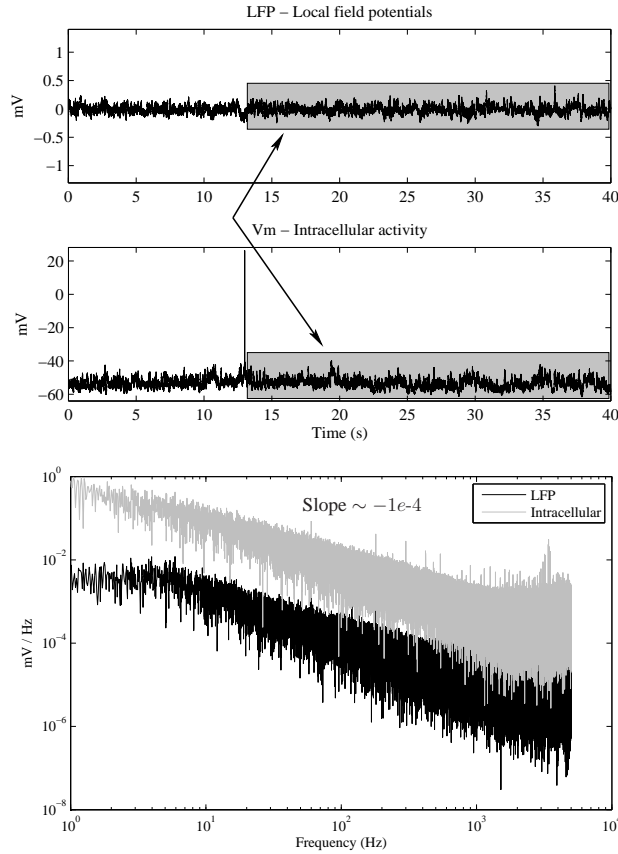


Fig. 3 Top panels depict the time series of simultaneous recorded LFP and V_m from rat barrel cortex with bipolar montage. The current applied to this particular neuron was of -10.65 nA. The shaded grey box indicate the time period where analysis is performed. Thus we avoid any possible spike interference as our theory is based on the regime of linear activity. The bottom panels are the calculated Power spectra of both LFP and V_m and show similar scaling.

theoretical finding is that the transfer function takes very different forms according to the type of frequency dependence of the extracellular medium, and thus could be used as a means to estimate which type of frequency dependence (if any) is most consistent with experiments. Second, we have provided a preliminary analysis indicating that in rat barrel cortex, the extracellular medium seems frequency dependent with a Warburg type impedance.

In a previous investigation [Bédard and Destexhe (2009)], we have shown theoretically that several physical phenomena can lead to frequency dependence of the extracellular medium: ionic diffusion and membrane polarization. The former predicts an impedance of Warburg type ($Z \sim 1/\sqrt{\omega}$), while the latter predicts a capacitive-type impedance ($Z \sim 1/\omega$). These two phenomena can also explain different experimental observations: the frequency dependent conductivity observed experimentally in brain tissue [Gabriel *et al.* (1996)] can be reproduced by a combination of these two mechanisms, while recent measurements from monkey cortex suggesting resistive medium [Logothetis *et al.* (2007)] can be explained by the fact that the influence of diffusion was avoided in that case. A Warburg type impedance can also

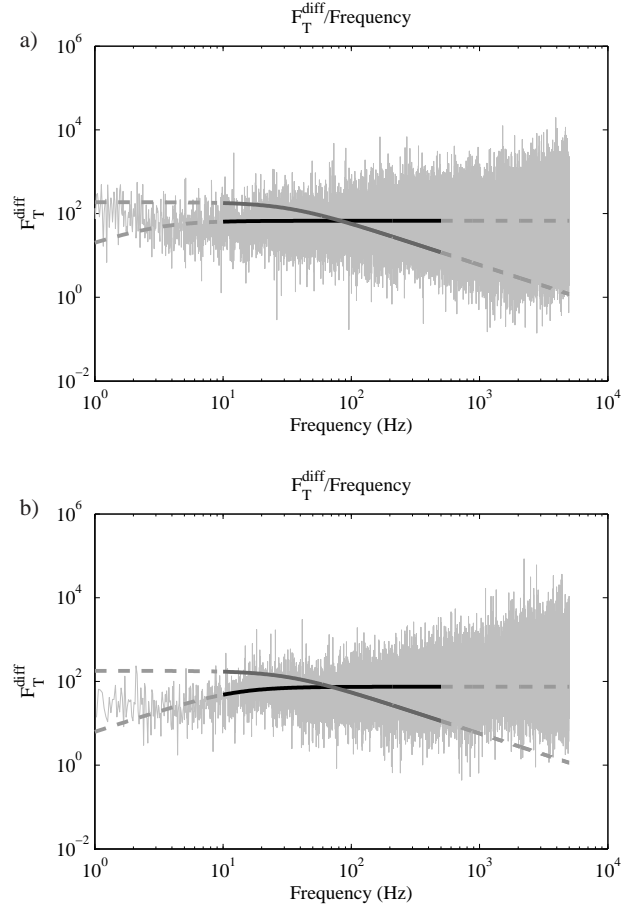


Fig. 4 Transfer function computed from experimental data by performing a ratio between the power spectra of intracellular and LFP activity. The top panel correspond to the data of Fig. 3 and the bottom panel to another cell. In both panels, the data transfer function $F_T^{(diff)}$ has an average slope of zero for frequencies between 10 and 500 Hz. However, we also note that data with longer periods of non occurrence of spikes as given by the example of Fig. 3 gives rise to data transfer function $F_T^{(diff)}$ with a better average. This is indicative that the theory explains the observed data. In addition, we perform a constrained nonlinear least square fit (Matlab) of Eq. 23 and Eq. 18 to the calculated data transfer function $F_T^{(diff)}$. This fit is performed between 0-500 Hz and the final fit is indicated by the solid black line (Warburg-type medium) and solid grey (Resistive medium) in both panels a and b. We observe a much better fit for the Warburg-type impedance with squared 2-norm of the residual of about $\sim 3.4 \times 10^2$, while for the resistive case we get $\sim 5 \times 10^3$. For panel a) we obtain for Eq. 23 a time constant of $\tau_m \approx 17.5$ ms, while for Eq. 18 we get close to the physiological limit of $\tau \approx 5$ ms. In panel b) we get similar scenario, where for Eq. 23 $\tau_m \approx 24$ ms and for Eq. 18 a $\tau \approx 5$ ms.

account for the $1/f$ power spectral structure of LFPs (see details in [Bédard and Destexhe (2009)]).

The present results are consistent with this analysis. The transfer functions measured here for 4 cells are all consistent with a Warburg type impedance of ionic diffusion. It is not consistent, however, with a resistive medium (see Fig. 4). Similarly, we did not need to invoke polarization phenomena to explain the transfer function between 5 and 500 Hz, suggesting that this phenomenon, if present, must play a role outside this frequency range, below 5 Hz. Fur-

ther theoretical and experimental work is needed to investigate this aspect.

It is important to note that the present technique does not suffer from the main limitation of direct measurements, in which artificially high currents interact with the medium very differently as natural sources. The present technique is only using physiological signals, with no current injection, and is therefore complementary to direct measurements.

Finally, the expression given by Eqs. 20 and 22 could be used to directly estimate the impedance of the extracellular medium as a function of frequency. We did not try this type of approach, but instead considered different hypotheses concerning the impedance of the medium. The preliminary observations reported here for 4 cells suggest that the medium is most consistent with a Warburg-type impedance, but further work would be necessary to provide a full estimate of the impedance spectrum of the medium. These results therefore must be considered as preliminary and must be confirmed by using a larger database of simultaneously recorded LFPs and intracellular recordings *in vivo*.

Appendix: impedance for non-ideal membranes

In this section, we derive the expressions for the impedance of non-ideal membranes, which take into account that the membrane capacitance cannot be charged instantaneously (see Bedard and Destexhe, 2008). Still within the linear regime and for a spherical source, we have:

$$I_r = \sum_{i=1}^N g_i(t, V_m)(V_m(t) - E_i)$$

$$I_c = C_m \frac{dV_c}{dt}$$

$$I_m = I_r + I_c$$

$$V_m = V_c + R_{MW} C_m \frac{dV_c}{dt} = V_c + \tau_{MW} \frac{dV_c}{dt}$$

where all parameters have the same definition as in the main text, except for r_{MW} , which is the Maxwell-Wagner resistance which gives the non-ideal aspect of the membrane capacitance. The associated time constant, τ_{MW} , is also known as “Maxwell-Wagner time”.

In the linear regime, we have

$$\begin{aligned} \Delta I_r &= \sum_{i=1}^N g_i \langle V_m \rangle_t \Delta V_m \\ \Delta I_c &= C_m \frac{d\Delta V_c}{dt} \end{aligned} \quad (26)$$

$$\Delta I_m = \Delta I_r + \Delta I_c$$

$$\Delta V_m = \Delta V_c + \tau_{MW} \frac{d\Delta V_c}{dt}$$

Thus, in these conditions, the system of equations associated to the membrane is linear with time-independent coefficients.

By expressing the variation of current produced by the cell as a function of the variation of membrane voltage, in Fourier space, we obtain:

$$\begin{aligned} \Delta I_r(\omega) &= G_m \Delta V_m(\omega) \\ \Delta I_c(\omega) &= i\omega C_m \Delta V_c(\omega) \\ \Delta I_m(\omega) &= \Delta I_r(\omega) + \Delta I_c(\omega) \\ \Delta V_m(\omega) &= \Delta V_c(\omega) + i\omega \tau_{MW} \Delta V_c(\omega) \end{aligned} \quad (27)$$

where

$$G_m = \sum_{i=1}^N g_i$$

It follows that the membrane impedance is given by:

$$Z_m(\omega) = \frac{\Delta V_m(\omega)}{\Delta I(\omega)} = \frac{R_m}{1 + i\omega \tau_{MW}} \quad (28)$$

where $R_m = \frac{1}{G_m}$. Note that if we set $\tau_{MW} = 0$, we recover the same expressions for the impedance of ideal membranes, as considered in the main text.

Acknowledgments

Research supported by the Centre National de la Recherche Scientifique (CNRS, France), Agence Nationale de la Recherche (ANR, France) and the Future and Emerging Technologies program (FET, European Union; FACETS project). Additional information is available at <http://cns.iaf.cnrs-gif.fr>

References

- Bédard *et al.* (2004). Bédard, C., Kröger, H., Destexhe, A. (2004). Modeling extracellular field potentials and the frequency-filtering properties of extracellular space. *Biophys. J.* **64**:1829-1842.
- Bédard and Destexhe (2008). Bédard, C., Destexhe, A. (2008). A modified cable formalism for modeling neuronal membranes at high frequencies. *Biophys. J.* **94**(4):1133-1143.
- Bédard and Destexhe (2009). Bédard, C., Destexhe, A. (2009). Macroscopic models of local field potentials and the apparent 1/f noise in brain activity. *Biophys. J.* **96**(7):2589-4608.
- Destexhe *et al.* (1999). Destexhe, A., Contreras D., Steriade, M. (1999). Spatiotemporal analysis of local field potentials and unit discharges in cat cerebral cortex during natural wake and sleep states. *J. Neurosci.* **19**:4595-4608.
- Erchova and McGonigle (2008). Erchova, I., McGonigle, D. J. (2008). Rhythms of the brain: An examination of mixed mode oscillation approaches to the analysis of neurophysiological data *Chaos* **18**:015115.
- Gabriel *et al.* (1996). Gabriel, S., Lau, R.W., Gabriel, C. (1996). The dielectric properties of biological tissues : II. Measurements in the frequency range 10 Hz to 20 GHz. *Phys. Med. Biol.* **41**:2251-2269.
- Jefferys (1995). Jefferys, J. G. R. (1995). Nonsynaptic modulation of neuronal activity in the brain: Electric currents and extracellular ions. *Physiological Reviews* **75** (4):689-714.
- Katzner *et al.* (2009). Katzner S., Nauhaus I., Benucci A., Bonin V., Ringach D. L., Carandini M. (2009). Local origin of field potentials in visual cortex. *Neuron* **61**:35-41.
- Logothetis *et al.* (2007). Logothetis, N. K., Kayser, C., Oeltermann, A. (2007). In vivo measurement of cortical impedance spectrum in monkeys: Implications for signal propagation. *Neuron* **55**:809-823.
- Chari and Salon (1999). Chari M.V.K. and S.J. Salon (1999), Numerical methods in electromagnetism, Academic Press
- Nunez and Srinivasan (2006). Nunez, P. L., Srinivasan, R. (2006) Electric Fields of the Brain: The neurophysics of EEG. *Oxford University Press, New York*.
- Ranck (1963). Ranck, J.B., Jr. (1963) Specific impedance of rabbit cerebral cortex. *Exp. Neurol.* **7**:144-152.